



## Numerical Simulation of Transient Air Flow and Particle Deposition in a Lung and Bronchus of a Human Respiratory System

A. R. Tahavvor<sup>1\*</sup>, P. Zarrinchang<sup>2</sup>

<sup>1</sup> Department of Mechanical Engineering, Shiraz Branch, Islamic Azad University, Shiraz, Iran

<sup>2</sup> Mechanical Engineering Group, Pardis College, Isfahan University of Technology, Isfahan, Iran

**ABSTRACT:** In the present study, the realistic model of the human trachea with five generations that are obtained from computerized tomography scan images is considered. Due to the complexity of lung geometry, many researchers have used simple models. Therefore in the present study realistic model with all geometrical details are considered. The airflow behavior, particle transport and deposition in various conditions such as steady flow, transient flow, light breathing and heavy breathing condition for various micro-particles diameters are investigated. Governing equations are solved and obtained results show that the flow patterns in the realistic model are much more complicated than those of symmetrical models. Also, the particle deposition pattern in the realistic condition is very different from that of the symmetrical model and the details of the trachea are very important and affect the deposition fractions in the small airways. Also, results show that the turbulent effect should be counted properly since the particle deposition in turbulent flow is 30 percent greater than the laminar flow and the dominant mechanism of micro-particle deposition is impaction and increasing of particles diameter, particle density, and the airflow rate leads to an increase of particle deposition.

### Review History:

Received: 2019-06-23

Revised: 2019-10-07

Accepted: 2019-12-09

Available Online: 2019-12-23

### Keywords:

Trachea

Lung

Respiratory system

Computational fluid dynamics

Micro-particle deposition

## 1. INTRODUCTION

The air entering the respiratory system of humans always has suspended particles of less than 100 micrometers. These particles either naturally enter the air stream or are produced by human activities, such as particles from the factories outlets and cars. Many medicines are also used as sprays. These particles travel and breathe through the airflow paths such as the nose, nasal passages, and trachea. A significant percentage of these particles are formed due to contact with the airway paths in different areas of the respiratory system and therefore affect the adjacent tissues [1-4].

Since 1990, with the development of Computerized Tomography (CT) scan technology and Computational Fluid Dynamics (CFD), studies have tended to be numerical approaches. Radiography also eliminates the problem of lack of access to the respiratory tract and provides appropriate models for this. Due to the complexity of the lung, many researchers have used simple models [5,6] but recently, with the advancement of high-resolution tomography and modern computer modeling techniques, researchers have used the accurate models close to the real lung shape [7-9].

Weibel [10] presented one of the first and most widely used models for lung simulation. In this model, the trachea is considered as the first branch (zero generation), and each branch is divided into two branches regularly up to the

branch 23 that leads to the air cavities. Despite its simplicity, this model is very popular, and many researchers have based their research on it. Luo et al. [11] simulate the particles in a blocked duct. For this purpose, they use a three-dimensional model with four divisions. The model has hexagonal cells and incompressible flow is solved in the duct using the CFD techniques. The results indicate that the area of the respiratory tract has the highest settling efficiency.

Feng and Kleinstreuer [12] reviewed the transfer and collision of micro-particles in three separate divisions of the human airway. The results of this study provide a way to accurately simulate the dynamics of aerosol particles in the lungs to improve the estimation of the respiratory dose of toxic particles. Freitas and Schröder [13] studied numerical flow in six stages of division of a 3Dimensional (3D) human lung model. The study is based on the Lattice-Boltzmann Method (LBM). They have shown that LBM is a suitable tool for simulating the flow structure in the human lungs. Gemci et al. [14] succeeded in modeling the 17 stages of a human respiratory system using the FLUENT software. The above model used an unstructured tetrahedral grid and steady airflow with a rate of 28.3 L.min<sup>-1</sup>. Also, the turbulent transient flow has been investigated by the Large-Eddy Simulation model. The results show that the nature of the secondary vortices of the flow in the asymmetric passages has a significant variation due to the anatomy of the passage.

\*Corresponding author's email: tahavvor@iaushiraz.ac.ir



Longest and Vinchurkar [15] have evaluated the effects of transient turbulent flow with suspended particles in the human respiratory passages. This study refers to the local meeting of particles in the division area in a turbulent stream. For better validation, the results of the two models are made. The first model is a laboratory and only includes the division area. The secondary model consists of the entire geometry of the passages. This model is simulated by CFD and the standard  $k-\omega$  model is used as a turbulence model. The results of the simulation model are in good agreement with the experimental results. Due to the difficulty in producing particles for experimental measurements, few studies have been conducted on the deposition of particles in the airway pathways of the human respiratory system, and in general, very little information is available for the transport of micro-particles during the respiratory cycle.

According to the previous researches in this area, an accurate simulation of transient and turbulent fluid flow with particle deposition in a realistic geometrical model has been not done yet. Therefore, in the present study, the model with the mentioned properties are considered and particles behavior under various flow conditions are investigated. Results of this study are suitable for researchers who are studying the risk of respiratory insufficiency of substances on the health as well as respiration and thinning of small drugs in the respiratory passages.

## 2. NUMERICAL MODEL

In all lung models, the main respiratory way in each branch is subdivided into two sub-branches, which are either symmetrically in one plane [10,16], or in the form of models symmetrically but not in one plane [17-19], and the best case, an asymmetric model derived from empirical observations [20-22]. In which the respiratory tract is modeled in the form of straight and cylindrical tubes that are connected with a specific length and diameter. The present study was carried out based on computerized radiography images of a 64 years old woman with a height of 165 cm, 52 kg in weight and without any problem in her respiratory system. The spiral imaging method is used with a total body scan with a peak of 120 kV and a wavelength of 99.00 mm. A CT-scan consists of a wide range of densities representing different tissues. A favorite tissue is determined by the threshold set in the geometry software. Under the supervision of specialists, the boundary between the mucus in the airways and the air in the upper respiratory passage is determined and considered in CT-scan images. Fig. 1 shows the transverse and coronal sections of the trachea and lungs. The final volume of the model generated from CT-scan images in different faces is shown in Fig. 2. The grid used in this simulation, Fig. 3, has 785000 nodes and has a skewness of 0.25. Transmission and deposition of particles are simulated at a rate of respiration of 15 and 60 L.min<sup>-1</sup> with particles of 3, 5 and 10 micrometers with different densities. Table 1 shows the properties of the air, and the solid particles respectively.

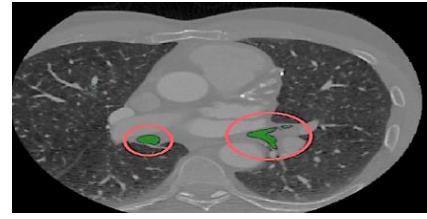


Fig. 1. Transverse and coronal sections of the trachea

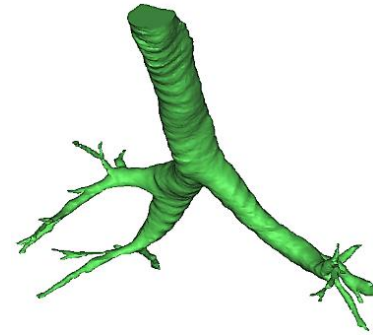


Fig. 2. Final volume of the model generated from CT-scan images of respiratory airway



Fig. 3. Generated grids used for modeling

## 3. BOUNDARY AND INITIAL CONDITIONS

At the inlet of the domain, the velocity inlet condition is used. In steady condition, the velocity considered as a constant value. Also, the boundary condition at the outlet due to the lack of information in this section is considered as an outflow condition [17,24]. This condition works more accurately when the flow is developed [25]. In transient conditions, the respiratory condition is considered for the volumetric flow rate of 15 L.min<sup>-1</sup> for normal breathing and 60 L.min<sup>-1</sup> for breathing in heavy activity. Also, the sinusoidal waveform is used for laminar and turbulent velocity profile as shown in Figs. 4 and 5 [21]. The airflow properties are summarized in Table 2 [26].

## 4. GOVERNING EQUATIONS

To determine the behavior of particles against the airflow, the Stokes number which represents the ratio of inertial force to drag force is used. Stokes number is defined as follows:

$$St = \frac{\rho_p d_p^2 U}{18 \mu d_c} \quad (1)$$

where  $\rho_p$ ,  $d_p$ ,  $U$ , and  $\mu$  are particle density, particle diameter, particle velocity and viscosity of fluid respectively.

**Table 1. Air and particle properties [15]**

Material	Density (kg.m <sup>-3</sup> )	Dynamic viscosity (kg.m <sup>-1</sup> .s <sup>-1</sup> )		Kinematic viscosity (m <sup>2</sup> .s <sup>-1</sup> )	
Air	1.225	1.7894×10 <sup>-5</sup>		1.46073×10 <sup>-5</sup>	
Physical state		Rest: 15 L.min <sup>-1</sup>		Heavy activity: 60 L.min <sup>-1</sup>	
Particle diameter (µm)		5	10	3	10
Particle density (kg.m <sup>-3</sup> .10 <sup>3</sup> )		1.06	8.29	1.06	5.75

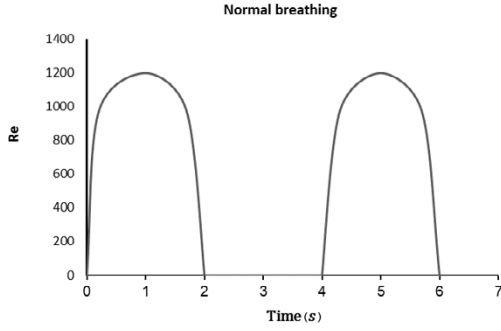


**Fig. 4. Sinusoidal velocity profile at rest [21]**

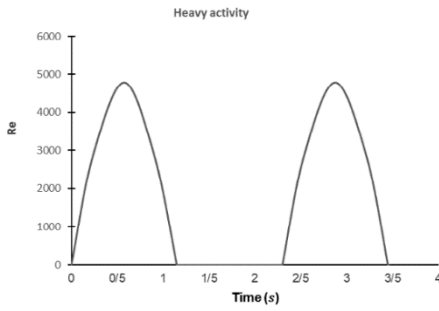


**Fig. 5. Parabolic velocity profile at heavy activity [21]**

Reynolds stress tensor respectively. The Reynolds Stress equation Model (RSM) turbulence model is employed in the present study to close the Reynolds-Averaged Navier-Stokes (RANS) equations according to the method that is described by reference [27]. It is being noted that summation notation  $i, j = 1, 2, 3$  demonstrate the  $x, y, z$  components of the velocity vector and the spatial coordinates. The particle size is selected in the range of 3 to 10 micrometers. In this range, gravitational effects are negligible. Also in the present study particle modification on fluids and collision between particles are neglected. ANSYS FLUENT<sup>®</sup> predicts the trajectory of a particle by integrating the force balance on the particle, which is written in a Lagrangian reference frame. This force balance equates the particle inertia with the forces acting on the particle. The accelerated velocity of the particle due to five forces, drag, gravitational, buoyancy, Brownian, and Saffman’s lift forces is considered and determined the particle deposition behavior as follows [27]:

$$\frac{du_p}{dt} = \frac{1}{\tau_p} \frac{C_D Re_p}{24} (u_g - u_p) + \frac{g(\rho_p - \rho_g)}{\rho_p} + \zeta \sqrt{\frac{\pi S_0}{\Delta t}} + \frac{2\rho K_c v^{0.5}}{\rho_p d_p (S_{lk} S_{kl})} S_{ij} (u_g - u_p) \tag{5}$$

These equations are used according to the method presented by Lu and Zhang [27].

**5. DISCRETIZATION SCHEME**

Governing equations are solved using an ANSYS FLUENT<sup>®</sup> 19 software which has the efficient to simulate the airflow into the airways. Also, an unstructured multi-block grid is used. This code uses the Pressure Implicit Splitting of Operators’ (PISO) algorithm and all variables of the flow are located at the centers of the control volumes. The 2<sup>nd</sup> order upwind scheme is employed to model the convective terms. In order to capture the viscous sublayer thickness, the generated grid has a high concentration near the walls. As a requirement of low Reynolds turbulent flow modeling, the first grid point above the wall is given a value of  $y^+ \leq 1$ .  $y^+ = \frac{u_\tau y}{\nu}$  and  $u_\tau$  are as follows:

$$u_\tau \equiv \sqrt{\frac{\tau_w}{\rho}} \tag{6}$$

Also, to simulate the accelerated velocity of the particle

Also, Reynolds number is defined as follows:

$$Re = \frac{\rho U D_h}{\mu} \tag{2}$$

where  $\rho, \mu, U,$  and  $D_h$  are air density, air viscosity, flow velocity and hydraulic diameter of passage respectively. Also, governing equations are as follows:

$$\frac{\partial u_i}{\partial x_i} = 0 \tag{3}$$

$$\frac{\partial \bar{u}_i}{\partial t} + \bar{u}_j \frac{\partial \bar{u}_i}{\partial x_j} = -\frac{1}{\rho} \frac{\partial \bar{p}}{\partial x_i} + \tag{4}$$

$$\frac{1}{\rho} \frac{\partial}{\partial x_j} \left( \mu \frac{\partial \bar{u}_i}{\partial x_j} - \rho \overline{u'_i u'_j} \right)$$

where  $u_i, p$  and  $\rho u'_i u'_j$  are the air velocity, pressure, and

**Table 2. Input transient form parameters and fluid properties for normal breathing [26]**

Physical state	Normal breathing	Heavy activity
Breathing rate ( $\text{min}^{-1}$ )	15	60
Breathing phase rate ( $t_{in}/t_{total}$ )	0.47	0.47
Respiration frequency Cycle ( $\text{min}^{-1}$ )	14	24.5
Reynolds number	1196	4785
Density ( $\text{kg.m}^{-3}$ )	1.225	1.225
Dynamic viscosity ( $\text{kg.m}^{-1}.s^{-1}$ )	$1.7894 \times 10^{-5}$	$1.7894 \times 10^{-5}$
Kinematic viscosity ( $\text{m}^2.s^{-1}$ )	$1.46073 \times 10^{-5}$	$1.46073 \times 10^{-5}$

**Table 3. Air flow grid Study**

Case	Number of nodes	Deflection coefficient (Best = 0)	Shear stress on the wall ( Pa )
1	176059	0.33431	0.2058911
2	202778	0.34428	0.2035427
3	412367	0.28580	0.2583323
4	785821	0.25532	0.2693441
5	1056057	0.24456	0.2674305
6	1543800	0.23597	0.2665389

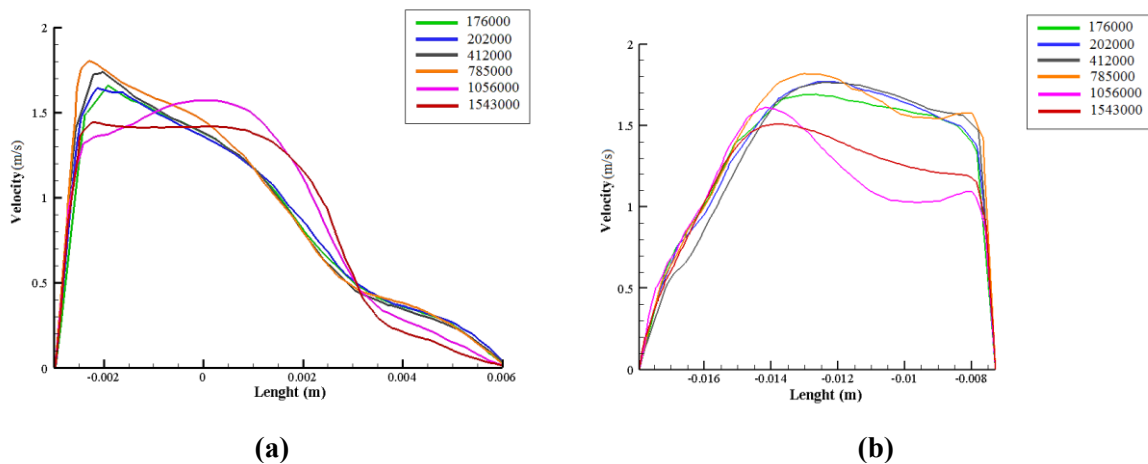


**Fig. 6. Velocity on the horizontal line in the a) left lung entrance, b) right lung entrance**

due to the mentioned five forces in section 4 and based on the method of Lu and Zhang [27], the User-Defined Function (UDF) is written and used in the simulation. Also, it is noted that convergence criteria are considered  $10^{-4}$  for all equations.

**6. RESULTS**

To select the optimal grid, six different grids with tetrahedral cells have been investigated. Summary of the grid study procedure is presented in Table 3. According to this table, the fourth grid size with 785821 nodes has been selected.

Also, fluid flow in these grids is compared with each other in terms of the profile of the velocity at the entrance of the left and right lungs in Figs. 6(a) and 6(b).

**6.1 Validation of results**

**6.1.1 Steady simulation**

Simulation of fluid flow is validated by comparing the

results in the left lung input section with the experimental data set provided by references [17-18, 28]. The steady velocity profile with the local Reynolds number 1196 that is shown in Fig. 7(a) is compared with the laboratory data of references [17-18, 28], which has a local Reynolds number of 1036 in Fig 7(b).

The R-square between numerical results and experimental data in Figs. 6 and 7 are 0.9883 and 0.9765 respectively which is showing very good agreement between obtained results and CT-scan data.

**6.1.2 Unsteady simulation**

Fig. 8 shows the comparison between the results of simulation of unsteady fluid velocity profile with the local Reynolds number 1196 at a time of 0.2 second and at the entrance to the left lung with the experimental data provided by references [17-19, 28], which has a local Reynolds number of 1036. The R-square between numerical results and experimental data in Fig. 8 is 0.9718 which is showing very good agreement

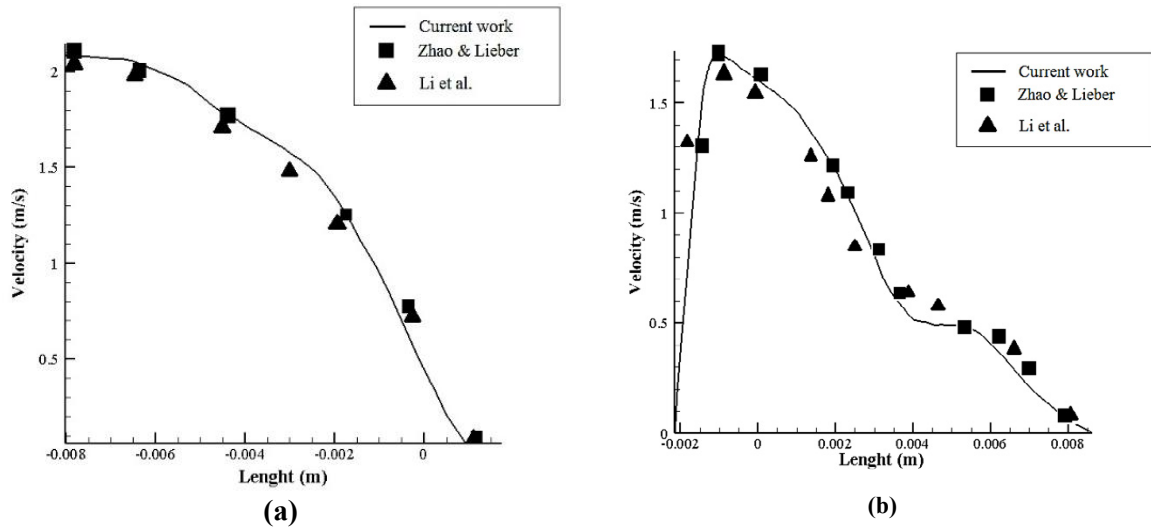


Fig. 7. Comparison of the axial velocity profile at the second stage of the lung with Li et al. [17,18] and Zhao and Lieber [28]

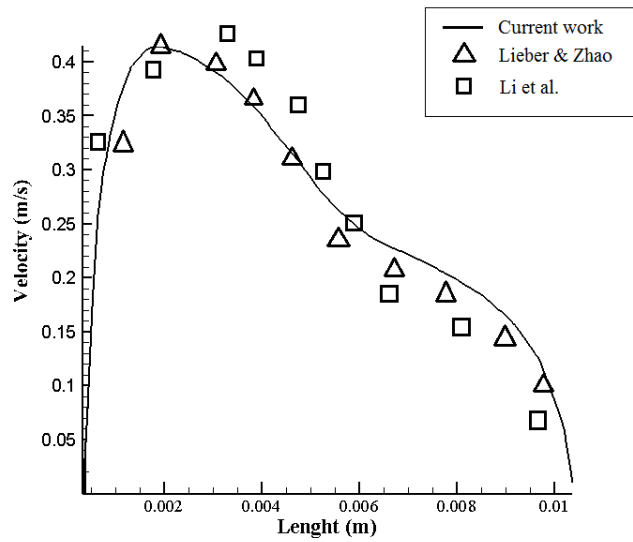


Fig. 8. Comparison of the velocity profile of the transient flow at the beginning of the second generation of the lung with reference [17-18, 28].

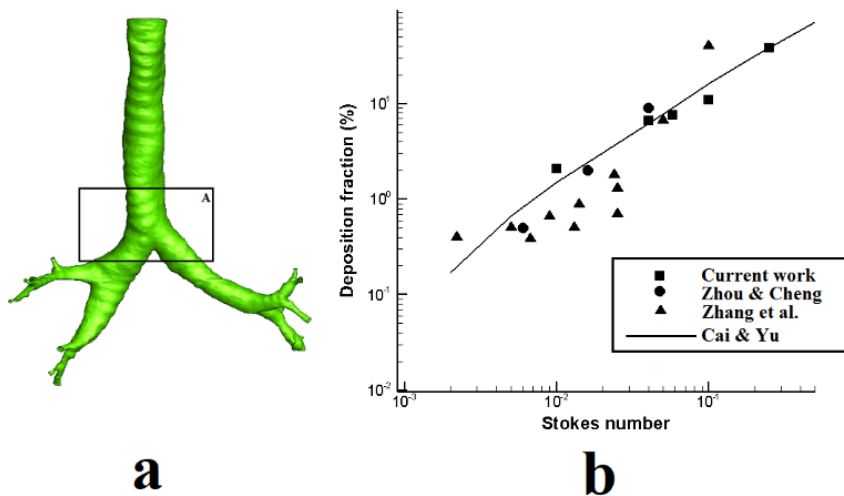


Fig. 9. a) Region located in the first generation of the trachea and lung. b) Comparison of deposition of fraction with reference [21].

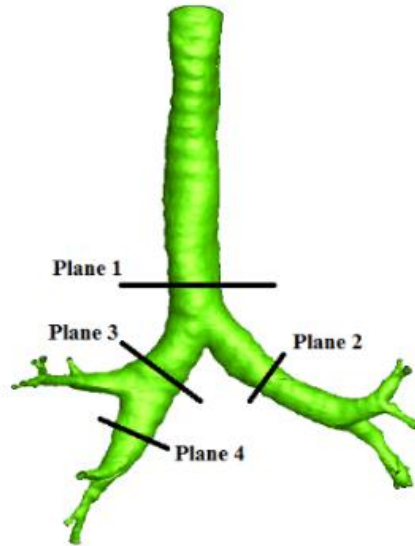


Fig. 10. The position of the planes used in simulation

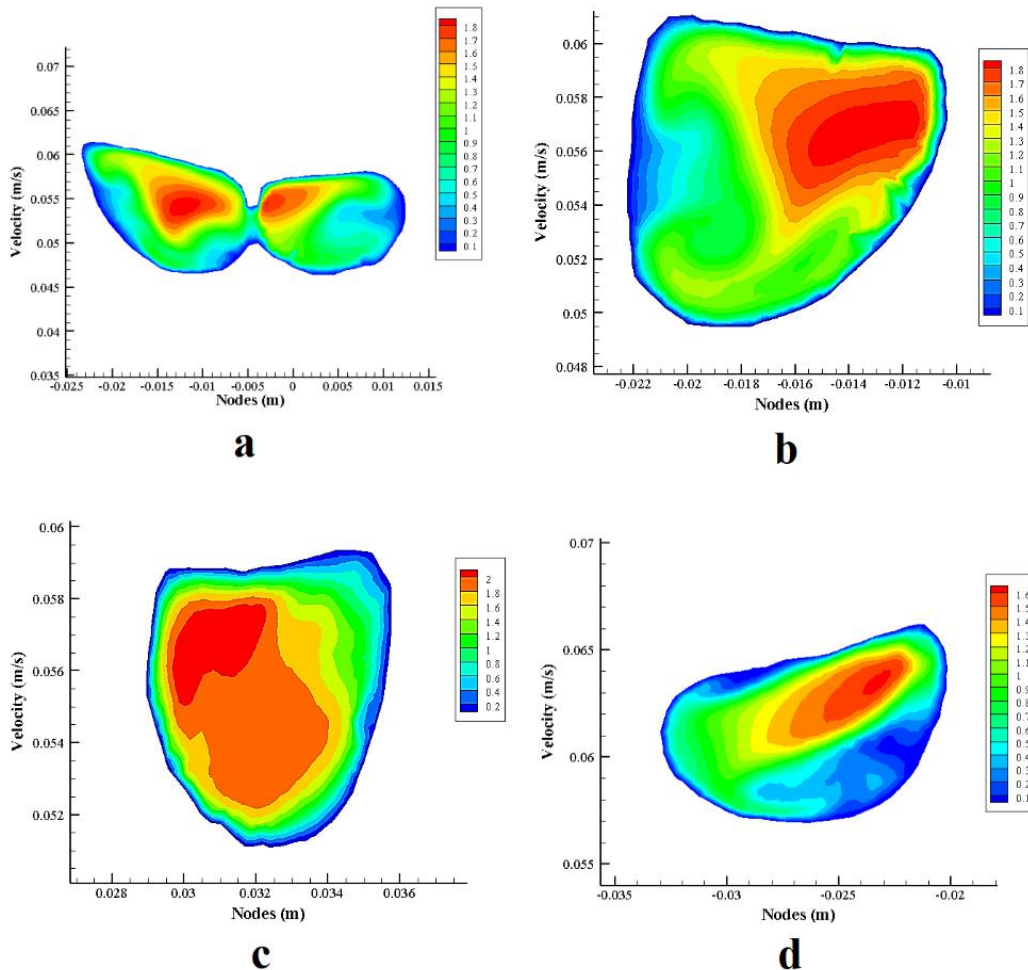


Fig. 11. Velocity contours in plane a) 1, b) 2, c) 3 and d) 4

between obtained results and CT-scan data.

### 6.1.3 Micro-particle deposition

To validate transfer and deposition of particles, obtained

results are compared with experimental and numerical data. The particle transfers and deposition in the region which is located in the first generation (shown in Fig. 9(a)) is compared in Fig. 9(b).

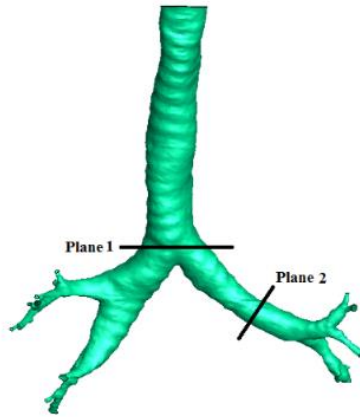


Fig. 12. The position of the planes used in simulation.

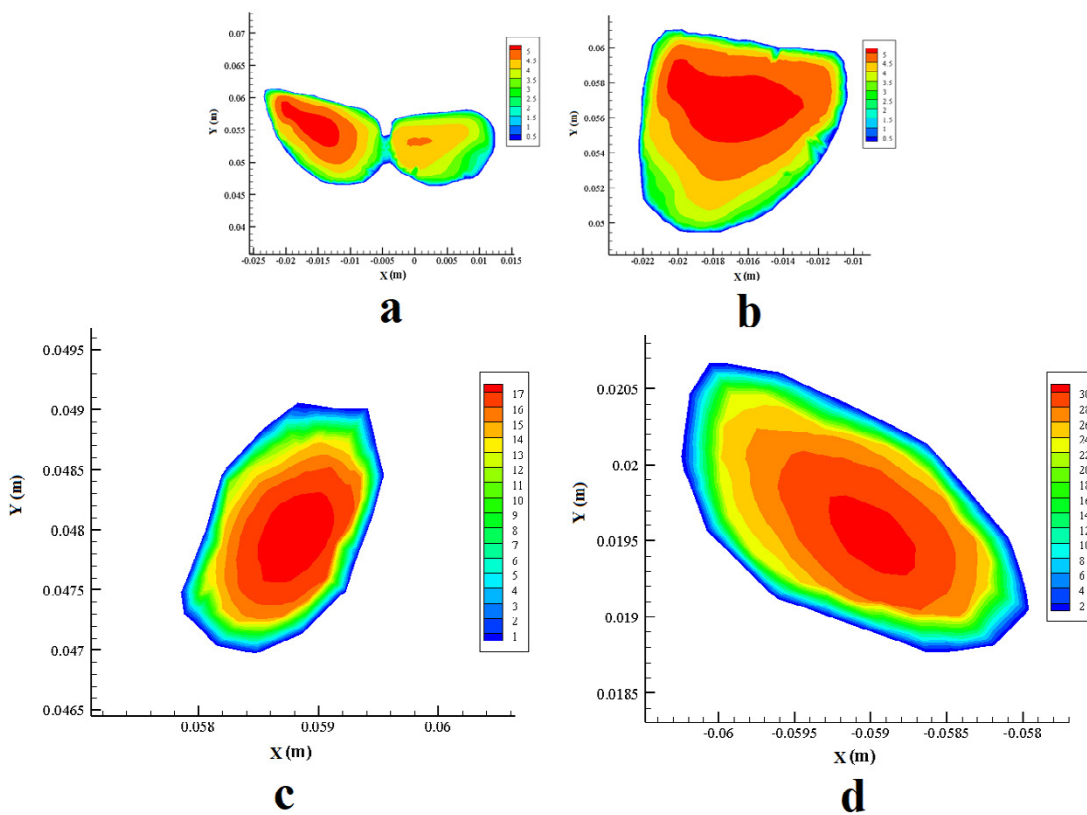


Fig. 13. Velocity contours in plane a) 1, b) 2, c) 3 and d) 4

The R-square between obtained results and experimental data in Fig. 9 is 0.8374 which is showing good agreement between obtained results and experimental data. The main reason for any differences between obtained results and other works is the difference in the shape and geometry of the air passages of this case from other cases.

## 6.2 Flow field

Results of flow field which are presented later show that airway resistance is the opposition to flow caused by the forces of friction. Resistance to flow in the airways depends on whether the flow is laminar or turbulent, on the

dimensions of the airway, and the viscosity of the gas. For laminar flow, resistance is quite low. That is, a relatively small driving pressure is needed to produce a certain flow rate. For turbulent flow, resistance is relatively large. That is, compared with laminar flow, a much larger driving pressure would be required to produce the same flow rate.

### 6.2.1 Steady laminar flow

The results of the steady laminar velocity field are presented in Fig. 11. For this purpose, four planes are considered at different levels as depicted in Fig. 10. In these cases, the volume flow rate of air is  $15 \text{ L}\cdot\text{min}^{-1}$  with the maximum

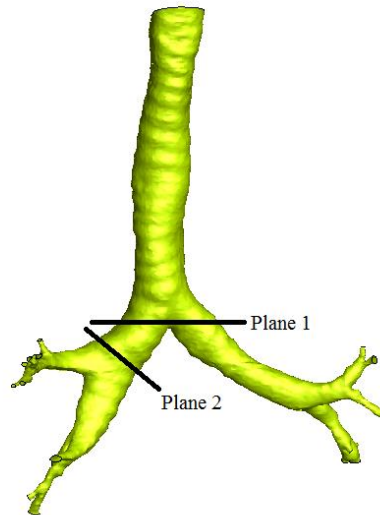


Fig. 14. The position of the planes used in simulation

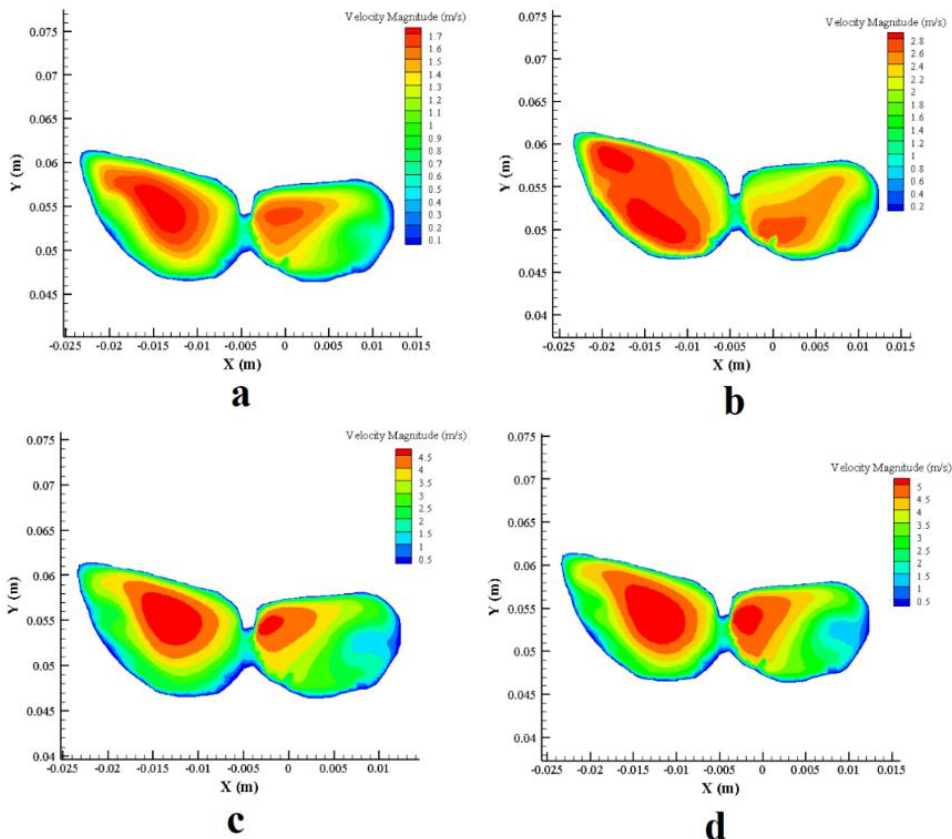


Fig. 15. Velocity contours in plane 1 after a) 0.2 s, b) 0.4 s, c) 0.6 s and d) 0.8 s

Reynolds number 1196 is considered. From the results, it can be observed that the fluid flow in each step is tended to the inner wall. The two eddy-shaped regions in Fig. 11(a) are due to the effect of the downstream flow and the flow between the two left and right lung incisions.

The velocity from the beginning of the air passage to the plane, which has a distance of about 95 mm from inlet increases by about 71% and to  $1.8 \text{ m}\cdot\text{s}^{-1}$ . Also, the maximum velocity in the right lung (Fig. 11(c)) is greater than 20% of the

left lung (Fig. 11(b)), due to the lower-left the ventral cross-section.

### 6.2.2 Steady turbulent flow

The results of the steady turbulent velocity field are presented in Fig. 13. For this purpose, some planes are considered at different levels as depicted in Fig. 12.

In these cases, the volume flow rate of air is  $60 \text{ L}\cdot\text{min}^{-1}$  with the maximum Reynolds number 4785 is considered.

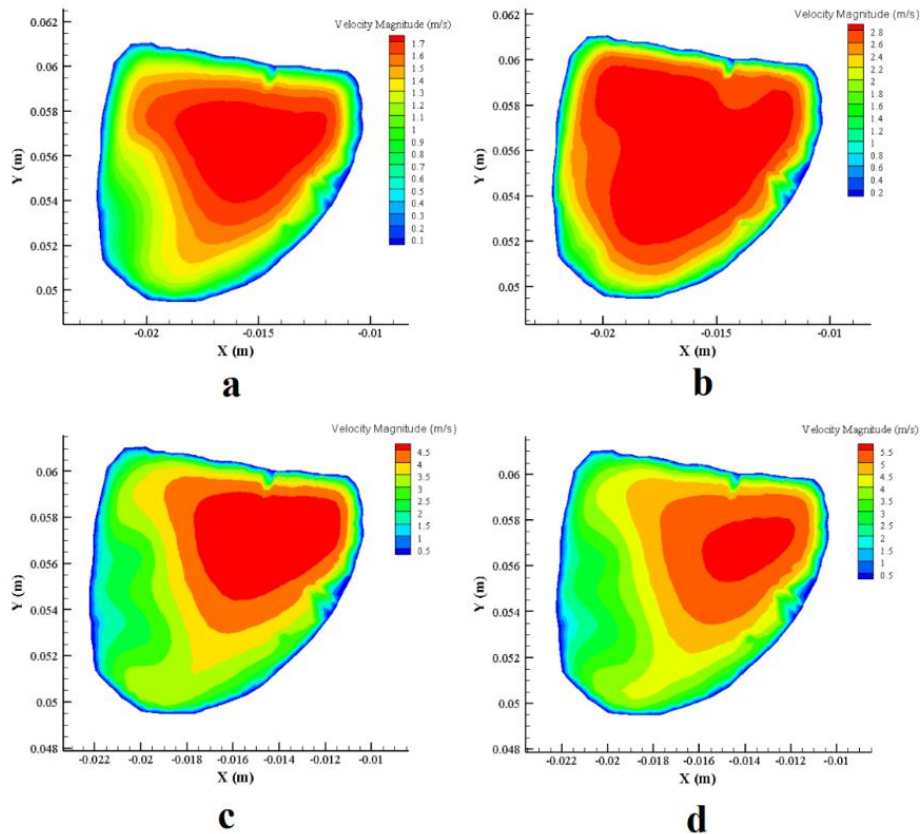


Fig. 16. Velocity contours in plane 2 after a) 0.2 s, b) 0.4 s, c) 0.6 s and d) 0.8 s

The two eddy-shaped regions in Fig. 13(a), which are due to the flow divide between the two cavities of the left/right lung, is observed. Also, increasing the flow rate along the air passage (95 mm) is about 19% and has reached about  $5 \text{ m.s}^{-1}$ .

### 6.2.3 Unsteady laminar flow

An unsteady laminar flow with a parabolic profile has been simulated in 10 time steps of 0.2 second. Planes 1 and 2 in Fig. 14 are selected to show results. In Figs. 15 and 16 velocity contours in time step 0.2, 0.4, 0.6 and 0.8 seconds are shown. As can be seen, increasing the time and, consequently, increasing the input velocity will increase the maximum speed at the desired level.

### 6.2.4 Unsteady turbulent flow

An unsteady turbulent flow with parabolic profile has been simulated in 10 time steps of 0.115 second. Planes 1 and 2 in Fig. 14 are selected to show results. In Figs. 17 and 18 velocity contours in time steps 0.115, 0.230, 0.345 and 0.460 seconds are shown. Similar to the laminar regime, increasing the time and, consequently, increasing the input velocity will increase the maximum speed at the desired level.

## 6.3 Particle transport and deposition

### 6.3.1 Steady laminar flow

Particle transport and deposition are simulated in the flow field with local Reynolds number 1196 at the entrance of the air passages and for particles of 5 and 10  $\mu\text{m}$  in diameter

with a density of 1060 and 8290  $\text{kg.m}^{-3}$ . Particle traces for above cases are shown in Figs. 19(a) to 19(d). Also, Table 4 shows the particle deposition results in the trachea and lung for the above-mentioned flow conditions. These results obtained from the particle summary that is reported by software and mentioned that which particles are escaped or trapped from or in the passages.

### 6.3.2 Steady turbulent flow

Particle transport and deposition are simulated in the turbulent flow field which is mentioned before for particles of 5 and 10  $\mu\text{m}$  in diameter with a density of 1060 and 5750  $\text{kg.m}^{-3}$ . Particle traces for above cases are shown in Figs. 20(a) to 20(d). Also, Table 5 shows the particle deposition results in the trachea and lung for the above-mentioned flow conditions. Results obtained from the particle summary that is reported by software and mentioned that which particles are escaped or trapped from or in the passages. A comparison between particle deposition in laminar and turbulent flow regime in steady condition shows that the laminar flow regime has not any considerable effect on particle deposition for particles of 3 and 5  $\mu\text{m}$  in diameter. But for particles of 10  $\mu\text{m}$  and density of 1060  $\text{kg.m}^{-3}$  turbulent flow increases particle deposition up to 27 percent.

### 6.3.3 Unsteady flow

Particle deposition in the unsteady situation is simulated in

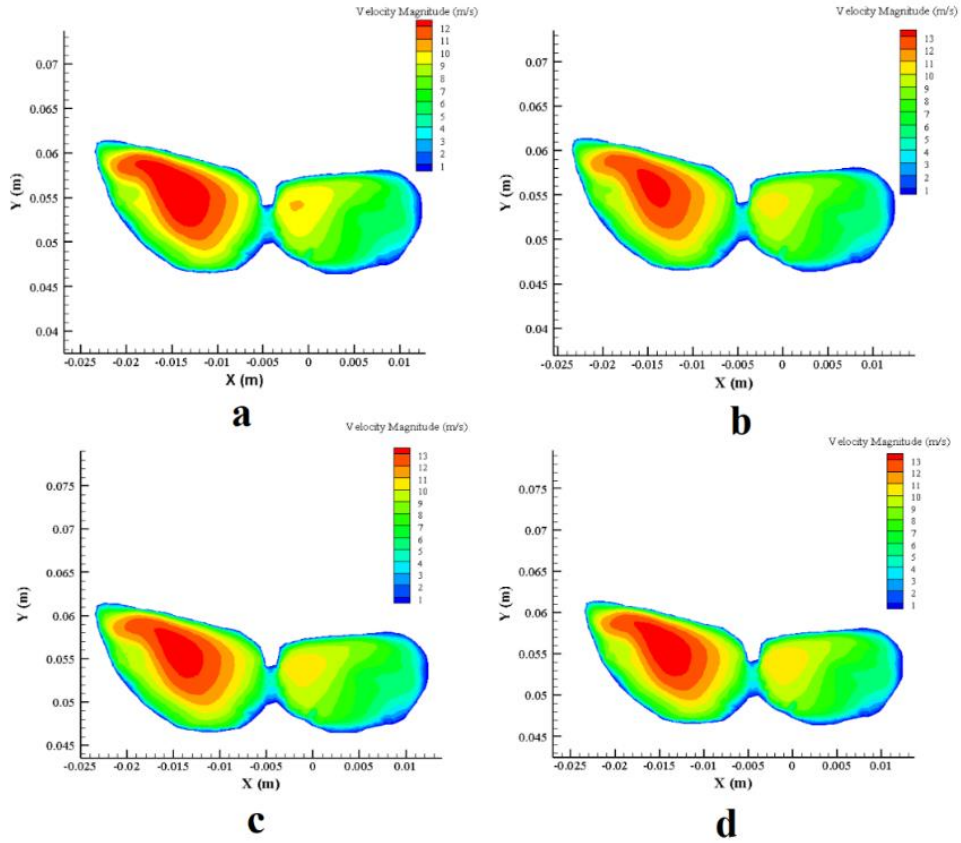


Fig. 17. Velocity contours in plane 1 after a) 0.115 s, b) 0.230 s, c) 0.345 and d) 0.460

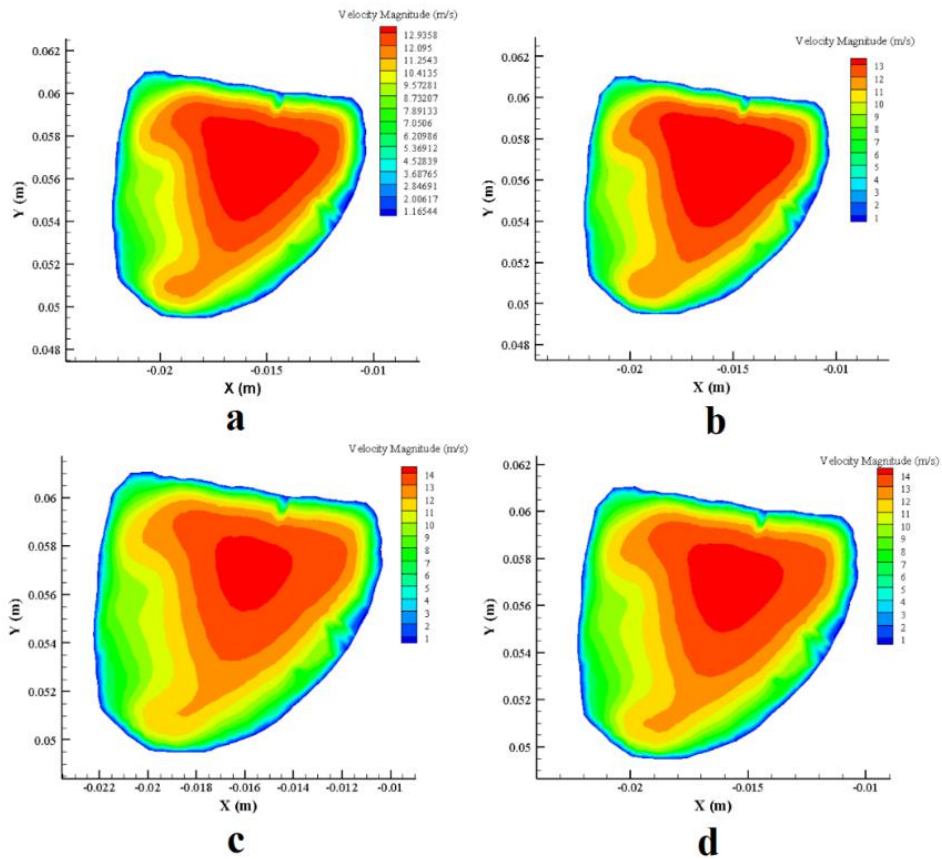


Fig. 18. Velocity contours in plane 2 after a) 0.115 s, b) 0.230 s, c) 0.345 and d) 0.460

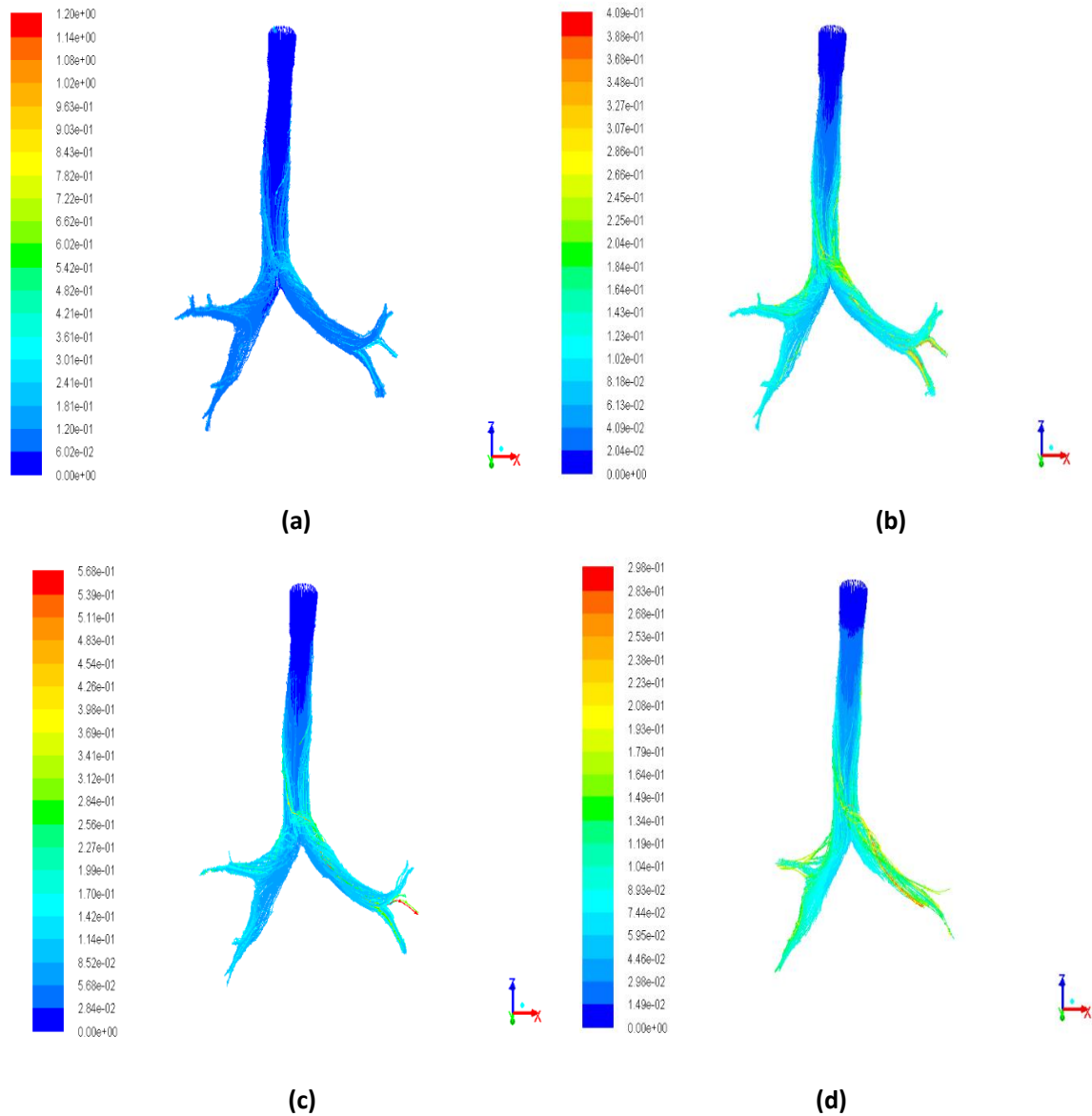


Fig. 19. Particle traces in laminar flow in steady condition colored by particle residence time in second (a)  $d_p = 5 \mu\text{m}$  and  $\rho_p = 1060 \text{ kg.m}^{-3}$ , (b)  $d_p = 10 \mu\text{m}$  and  $\rho_p = 1060 \text{ kg.m}^{-3}$ , (c)  $d_p = 5 \mu\text{m}$  and  $\rho_p = 8290 \text{ kg.m}^{-3}$ , (d)  $d_p = 10 \mu\text{m}$  and  $\rho_p = 8290 \text{ kg.m}^{-3}$

Table 4. Percentage of particles deposition in the trachea and lung of the tract for a steady and laminar air flow

Density ( $\text{kg.m}^{-3}$ )	Particle diameter	
	5 $\mu\text{m}$	10 $\mu\text{m}$
1060	38	66
8290	84	98

the laminar and turbulent regimes of flow with the mentioned conditions and time steps. Particle traces for unsteady flow for the laminar regime in 0.2 s and the turbulent regime in 0.115 s are shown in Figs. 21 and 22 respectively. Results of these situations are presented in Tables 6 and 7. Results of Tables 6 and 7 are obtained from the particle summary that is reported

by software and mentioned that which particles are escaped or trapped from or in the passages in each time step.

A comparison between particle deposition in laminar and turbulent regimes in unsteady condition show that similar to steady flow regimes, particles of 3 and 5  $\mu\text{m}$  in diameter deposition have not any considerable difference in laminar and turbulent flows. But for particles of 10  $\mu\text{m}$  and density of 1060  $\text{kg.m}^{-3}$  unsteady turbulent flow increases particle deposition about 35 to 55 percent.

## 7. CONCLUSIONS

The present study was carried out to investigate the airflow and transfer and deposition of micro-particles in the trachea and first to the fifth generation of lung passages in the respiratory system of a human. For this purpose, an accurate human lung model has been developed with the help

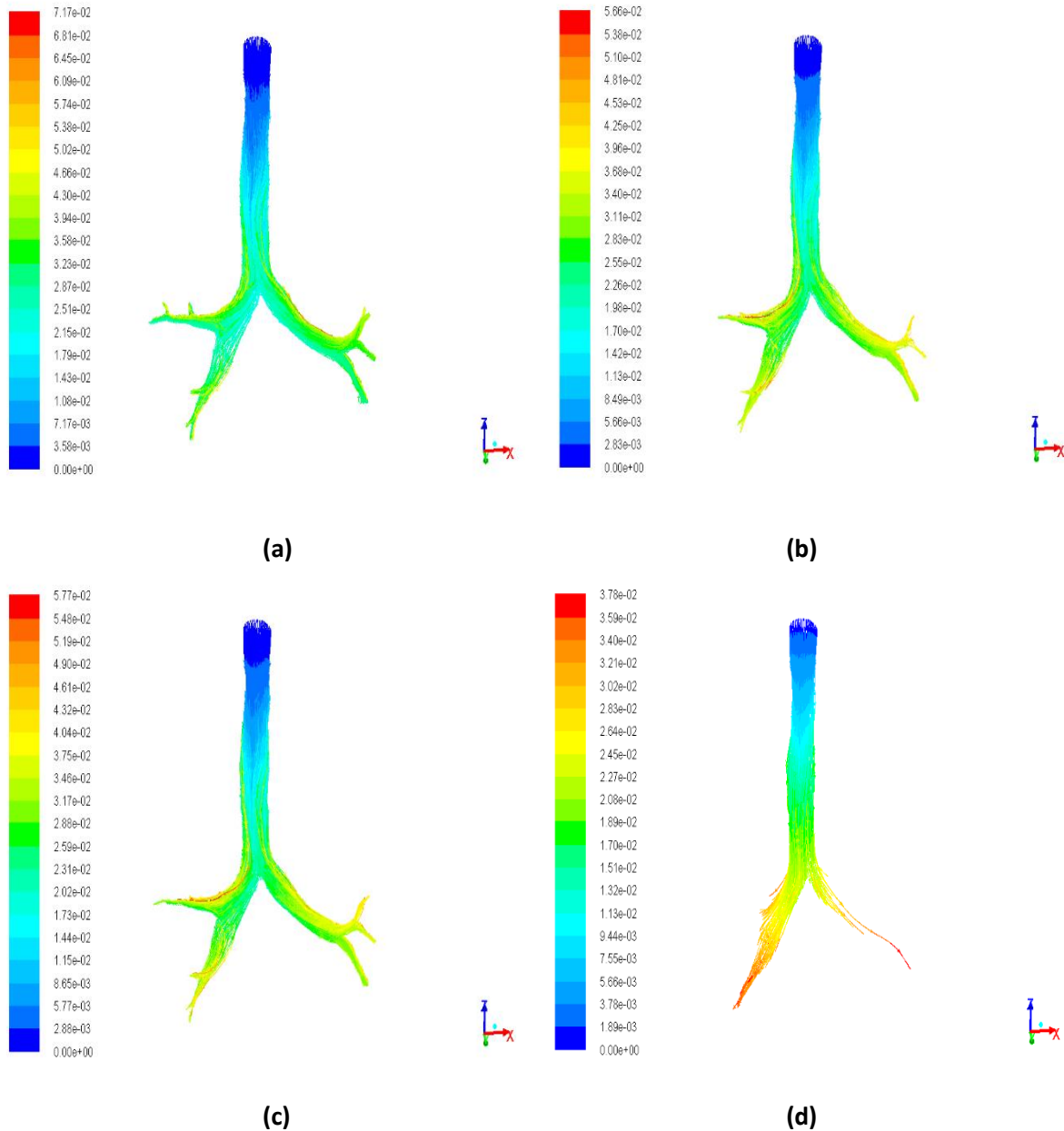


Fig. 20. Particle traces in turbulent flow in steady condition colored by particle residence time in second (a)  $d_p = 3 \mu\text{m}$  and  $\rho_p = 1060 \text{ kg.m}^{-3}$ , (b)  $d_p = 10 \mu\text{m}$  and  $\rho_p = 1060 \text{ kg.m}^{-3}$ , (c)  $d_p = 3 \mu\text{m}$  and  $\rho_p = 5750 \text{ kg.m}^{-3}$ , (d)  $d_p = 10 \mu\text{m}$  and  $\rho_p = 5750 \text{ kg.m}^{-3}$

Table 5. Percentage of particles deposition in the trachea and lung of the tract for a steady and turbulent air flow

Density ( $\text{kg.m}^{-3}$ )	Particle diameter	
	3 $\mu\text{m}$	10 $\mu\text{m}$
1060	32	91
5750	77	92

of CT-scan images. Following results are concluded from this research:

- The generated model of CT-scan images of the trachea and lung have much more complex flow pattern than other simulated simplified models.
- Tetrahedral cells which are used as lung grid cells present

satisfactory results.

- The change in velocity in the steady laminar case from an inlet to the end of the trachea is 71%.
- The maximum velocity in the steady condition at the entrance to the right lobe is more than 20% of the left lobe.
- The particle deposition increased with increasing of particle diameter. Therefore, as physiological observations in the medical sciences confirm that a portion of the nano- and micro-particles can sit in the respiratory system, and another part escapes toward the end of the lung and lower respiratory system.
- The turbulent flow pattern is different than the laminar flow pattern. The secondary flow in turbulent flow seems weaker than the laminar flow, and the turbulent axial speed in

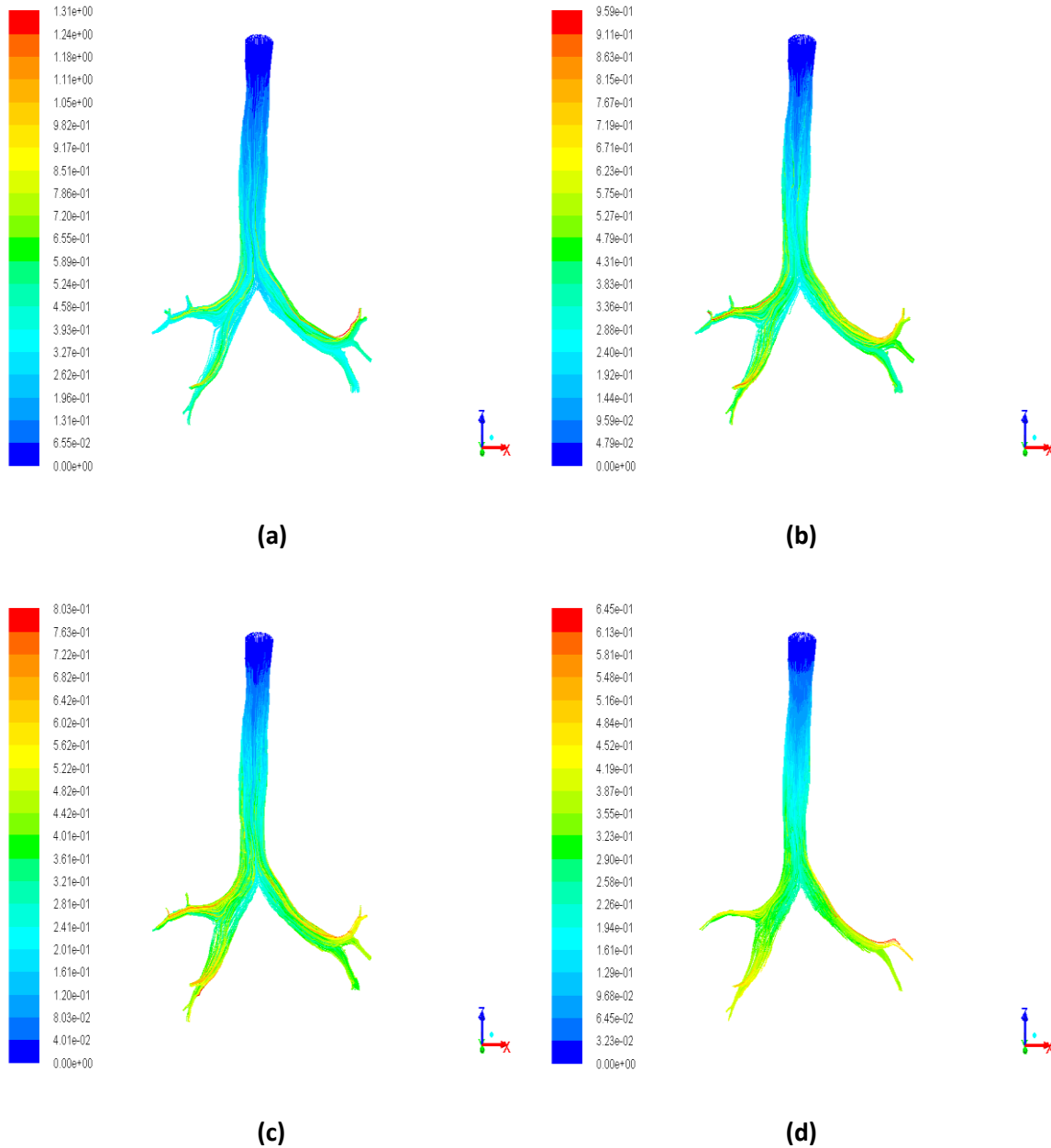


Fig. 21. Particle traces in laminar regime in unsteady condition colored by particle residence time in second in 0.2 s (a)  $d_p = 5 \mu\text{m}$  and  $\rho_p = 1060 \text{ kg.m}^{-3}$ , (b)  $d_p = 10 \mu\text{m}$  and  $\rho_p = 1060 \text{ kg.m}^{-3}$ , (c)  $d_p = 5 \mu\text{m}$  and  $\rho_p = 8290 \text{ kg.m}^{-3}$ , (d)  $d_p = 10 \mu\text{m}$  and  $\rho_p = 8290 \text{ kg.m}^{-3}$

Table 6. Percentage of particles deposition in the trachea and lung of tract for a transient and laminar air flow

Particle diameter		5 $\mu\text{m}$		10 $\mu\text{m}$	
Density ( $\text{kg.m}^{-3}$ )		1060	8290	1060	8290
Time step (s)	0.2	12	50	27	92
	0.4	16	63	44	93
	0.6	18	71	50	96
	0.8	21	76	55	97

Table 7. Percentage of particles deposition in the trachea and lung of tract for a transient and turbulent air flow

Particle diameter		3 $\mu\text{m}$		10 $\mu\text{m}$	
Density ( $\text{kg.m}^{-3}$ )		1060	5750	1060	5750
Time step (s)	0.115	13	41	61	97
	0.23	19	59	82	98
	0.345	21	70	88	100
	0.46	28	72	91	100

the center of the passage looks smoother.

- The flow rate of the entrance to the right lobe has

increased by about 20% relative to the left lobe in the turbulent stream compared to the laminar flow. So the deposition of

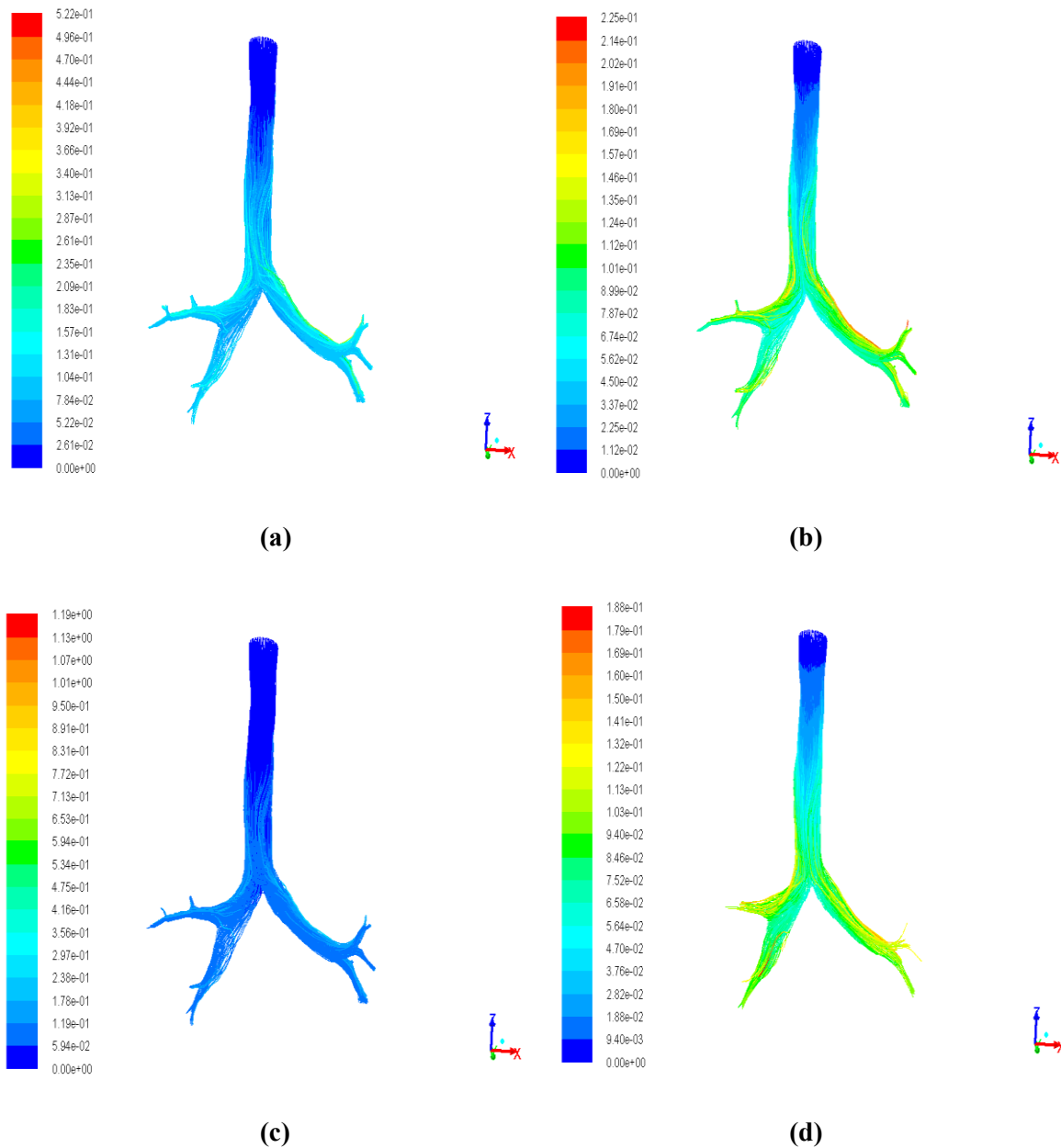


**Fig. 22. Particle traces in turbulent flow regime in unsteady condition colored by particle residence time in second in 0.115 s (a)  $d_p = 3 \mu\text{m}$  and  $\rho_p = 1060 \text{ kg.m}^{-3}$ , (b)  $d_p = 10 \mu\text{m}$  and  $\rho_p = 1060 \text{ kg.m}^{-3}$ , (c)  $d_p = 3 \mu\text{m}$  and  $\rho_p = 5750 \text{ kg.m}^{-3}$ , (d)  $d_p = 10 \mu\text{m}$  and  $\rho_p = 5750 \text{ kg.m}^{-3}$**

particles or drugs can be done more in the right lobe.

- The change in velocity in steady turbulent flow from an inlet to the end of the trachea is about 19%.

- The pattern of particle deposition in the realistic model of trachea and lung is completely different from the previous simple and symmetrical model. The roughness of the wall of passages has a significant effect on the particle transport, thus, they can trap a large proportion of particles and play an important role in the particle deposition in next generations and smaller airways.

- Changing the profile of the flow from steady to unsteady not only changes the flow pattern in the trachea but also changes the pattern of flow in all sub-branches. However, these changes are lower due to geometric complexities,

because geometry plays an important role in creating a developed local airflow.

- The effect of turbulence in the particle deposition should be taken into account since the particle deposition in a turbulent flow is about 30% more than that laminar flow.

- A comparison between particle deposition in laminar and turbulent flow regime in steady condition shows that the laminar flow regime has not any considerable effect on particle deposition for particles of 3 and 5  $\mu\text{m}$  in diameter. But for particles of 10  $\mu\text{m}$  and density of 1060  $\text{kg.m}^{-3}$  turbulent flow increases particle deposition up to 27 percent.

- A comparison between particle deposition in laminar and turbulent regimes in unsteady condition show that similar to steady flow regimes, particles of 3 and 5  $\mu\text{m}$  in

diameter deposition have not any considerable difference in laminar and turbulent flows. But for particles of 10  $\mu\text{m}$  and density of 1060  $\text{kg}\cdot\text{m}^{-3}$  unsteady turbulent flow increases particle deposition about 35 to 55 percent.

## REFERENCES

- [1] P. Gehr, J. Heyder, Particle-lung interactions, CRC Press, 2000.
- [2] J.Y. Park, S. Park, T.S. Lee, Y.H. Hwang, J.Y. Kim, W.J. Kang, J. Key, Biodegradable micro-sized discoidal polymeric particles for lung-targeted delivery system, *Biomaterials*, 218 (2019) 119331.
- [3] H. Calmet, G. Houzeaux, M. Vázquez, B. Eguzkitza, A. Gambaruto, A. Bates, D. Doorly, Flow features and micro-particle deposition in a human respiratory system during sniffing, *Journal of Aerosol Science*, 123 (2018) 171-184.
- [4] J. Watanabe, M. Watanabe, Anatomical factors of human respiratory tract influencing volume flow rate and number of particles arriving at each bronchus, *Biocybernetics and Biomedical Engineering*, 39(2) (2019) 526-535.
- [5] M. Rahimi-Gorji, O. Pourmehran, M. Gorji-Bandpy, T. Gorji, CFD simulation of airflow behavior and particle transport and deposition in different breathing conditions through the realistic model of human airways, *Journal of Molecular Liquids*, 209 (2015) 121-133.
- [6] Y. Kim, Z. Tong, H. Chan, R. Yang, CFD modelling of air and particle flows in different airway models, *Journal of Aerosol Science*, 134 (2019) 14-28.
- [7] A. Li, G. Ahmadi, Computer simulation of particle deposition in the upper tracheobronchial tree, *Aerosol science and technology*, 23(2) (1995) 201-223.
- [8] S. Kecorius, L. Madueño, J. Löndahl, E. Vallar, M.C. Galvez, L.F. Idolor, M. Gonzaga-Cayetano, T. Müller, W. Birmili, A. Wiedensohler, Respiratory tract deposition of inhaled roadside ultrafine refractory particles in a polluted megacity of South-East Asia, *Science of the Total Environment*, 663 (2019) 265-274.
- [9] W. Yan, C. Tang, Y. Liu, G. Li, Numerical study on abnormal airflow patterns and particle deposition characteristics in the realistic HUA model with pharyngeal obstruction, *Powder Technology*, 356 (2019) 148-161.
- [10] E.R. Weibel, Geometry and dimensions of airways of conductive and transitory zones, in: *Morphometry of the human lung*, Springer, 1963, pp. 110-135.
- [11] H. Luo, Y. Liu, X. Yang, Particle deposition in obstructed airways, *Journal of Biomechanics*, 40(14) (2007) 3096-3104.
- [12] Y. Feng, C. Kleinstreuer, Micron-particle transport, interactions and deposition in triple lung-airway bifurcations using a novel modeling approach, *Journal of Aerosol Science*, 71 (2014) 1-15.
- [13] R.K. Freitas, W. Schröder, Numerical investigation of the three-dimensional flow in a human lung model, *Journal of Biomechanics*, 41(11) (2008) 2446-2457.
- [14] T. Gemci, V. Ponyavin, Y. Chen, H. Chen, R. Collins, Computational model of airflow in upper 17 generations of human respiratory tract, *Journal of Biomechanics*, 41(9) (2008) 2047-2054.
- [15] P.W. Longest, S. Vinchurkar, Validating CFD predictions of respiratory aerosol deposition: effects of upstream transition and turbulence, *Journal of biomechanics*, 40(2) (2007) 305-316.
- [16] H.-C. Yeh, G. Schum, Models of human lung airways and their application to inhaled particle deposition, *Bulletin of mathematical biology*, 42(3) (1980) 461-480.
- [17] Z. Li, C. Kleinstreuer, Z. Zhang, Particle deposition in the human tracheobronchial airways due to transient inspiratory flow patterns, *Journal of aerosol science*, 38(6) (2007) 625-644.
- [18] Z. Li, C. Kleinstreuer, Z. Zhang, Simulation of airflow fields and microparticle deposition in realistic human lung airway models. Part I: Airflow patterns, *European Journal of Mechanics-B/Fluids*, 26(5) (2007) 632-649.
- [19] H. Jin, J. Fan, M. Zeng, K. Cen, Large eddy simulation of inhaled particle deposition within the human upper respiratory tract, *Journal of Aerosol Science*, 38(3) (2007) 257-268.
- [20] K. Horsfield, G. Cumming, Morphology of the bronchial tree in man, *Journal of applied physiology*, 24(3) (1968) 373-383.
- [21] Z. Zhang, C. Kleinstreuer, C. Kim, Cyclic micron-size particle inhalation and deposition in a triple bifurcation lung airway model, *Journal of Aerosol Science*, 33(2) (2002) 257-281.
- [22] Z. Zhang, C. Kleinstreuer, Airflow structures and nano-particle deposition in a human upper airway model, *Journal of computational physics*, 198(1) (2004) 178-210.
- [23] Z. Zhang, C. Kleinstreuer, Computational analysis of airflow and nanoparticle deposition in a combined nasal-oral-tracheobronchial airway model, *Journal of Aerosol Science*, 42(3) (2011) 174-194.
- [24] A.R. Tahavvor, P. Zarrinchang, S. Heidari, Numerical simulation of turbulent airflow in a human upper respiratory system, *Modares Mechanical Engineering*, 14(15) (2015) 267-272.
- [25] P.W. Longest, C. Kleinstreuer, J.R. Buchanan, Efficient computation of micro-particle dynamics including wall effects, *Computers & Fluids*, 33(4) (2004) 577-601.
- [26] C.S. Kim, L. Garcia, Particle deposition in cyclic bifurcating tube flow, *Aerosol Science and Technology*, 14(3) (1991) 302-315.
- [27] H. Lu, L.-z. Zhang, Particle Deposition Characteristics and Efficiency in Duct Air Flow over a Backward-Facing Step: Analysis of Influencing Factors, *Sustainability*, 11(3) (2019) 751.
- [28] Y. Zhao, B.B. Lieber, Steady inspiratory flow in a model symmetric bifurcation, *Journal of biomechanical engineering*, 116(4) (1994) 488-496.

### HOW TO CITE THIS ARTICLE

A.R. Tahavvor, P. Zarrinchang, *Numerical Simulation of Transient Air Flow and Particle Deposition in a Lung and Bronchus of a Human Respiratory System*, *AUT J. Mech Eng.*, 4(3) (2020) 347-362.

DOI: [10.22060/ajme.2019.16631.5830](https://doi.org/10.22060/ajme.2019.16631.5830)



